

2-Point Correlations in the *COBE*¹ DMR 4-Year Anisotropy Maps

G. Hinshaw^{2,3}, A.J. Banday^{2,4}, C.L. Bennett⁵, K.M. Górski^{2,6}, A. Kogut²,
C.H. Lineweaver⁷, G.F. Smoot^{8,9} & E.L. Wright¹⁰

ABSTRACT

The 2-point temperature correlation function is evaluated from the 4-year *COBE* DMR microwave anisotropy maps. We examine the 2-point function, which is the Legendre transform of the angular power spectrum, and show that the data are statistically consistent from channel to channel and frequency to frequency. The most likely quadrupole normalization is computed for a scale-invariant power-law spectrum of CMB anisotropy, using a variety of data combinations. For a given data set, the normalization inferred from the 2-point data is consistent with that inferred by other methods. The smallest and largest normalization deduced from any data combination are 16.4 and 19.6 μK respectively, with a value $\sim 18 \mu\text{K}$ generally preferred.

Subject headings: cosmic microwave background — cosmology: observations

¹The National Aeronautics and Space Administration/Goddard Space Flight Center (NASA/GSFC) is responsible for the design, development, and operation of the Cosmic Background Explorer (*COBE*). Scientific guidance is provided by the *COBE* Science Working Group. GSFC is also responsible for the development of the analysis software and for the production of the mission data sets.

²Hughes STX Corporation, Laboratory for Astronomy and Solar Physics, Code 685, NASA/GSFC, Greenbelt MD 20771.

³e-mail: hinshaw@stars.gsfc.nasa.gov

⁴Current address: Max Planck Institut für Astrophysik, 85740 Garching Bei München, Germany.

⁵Laboratory for Astronomy and Solar Physics, Code 685, NASA/GSFC, Greenbelt MD 20771.

⁶On leave from Warsaw University Observatory, Aleje Ujazdowskie 4, 00-478 Warszawa, Poland.

⁷Observatoire de Strasbourg, 67000, Strasbourg, France.

⁸Department of Physics, U.C. Berkeley, Berkeley CA 94720.

⁹Lawrence Berkeley Laboratory, Bldg 50-351, University of California, Berkeley CA 94720.

¹⁰UCLA Astronomy, P.O. Box 951562, Los Angeles CA 90095-1562.

1. Introduction

The detection of large angular scale anisotropies in the Cosmic Microwave Background (CMB) radiation was first reported by the *COBE*-DMR experiment in 1992 (Smoot et al. 1992; Bennett et al. 1992; Wright et al. 1992; Kogut et al. 1992). The initial detection was based only on the first year of flight data. Since that time the DMR Team processed and analyzed the first two years of data and found results to be consistent with the first year results (Bennett et al. 1994, Górski et al. 1994, Wright et al. 1994). We have now processed and analyzed the full 4-years of DMR observations: this paper is one of a series describing the results of our analysis. The maps and an overview of the scientific results are given in Bennett et al. (1996).

In this paper we analyze the anisotropy in the 4-year DMR maps using the 2-point correlation function as a measure of the angular power spectrum. The *COBE*-DMR experiment was designed to measure the CMB anisotropy on angular scales of $\geq 7^\circ$, corresponding to spherical harmonic multipole moments of order $\ell \lesssim 30$. The DMR has produced full-sky maps of the CMB temperature at each of three frequencies, 31.5, 53, and 90 GHz, with two independent channels, A and B, at each frequency. In principal, one can obtain an estimate of the CMB power spectrum from an anisotropy map simply by decomposing the map, $T(\theta, \phi)$, into spherical harmonic components and averaging them to find the mean power per mode ℓ : $T(\theta, \phi) = \sum_{\ell, m} a_{\ell m} Y_{\ell m}(\theta, \phi)$ with power spectrum $a_\ell^2 = \frac{1}{2\ell+1} \sum_{m=-\ell}^{\ell} |a_{\ell m}|^2$. In practice, however, there are a number of complications that arise. First, the need to apply a galactic cut to the data renders the spherical harmonics non-orthogonal, thereby coupling the $a_{\ell m}$ coefficients and increasing their uncertainty. Moreover, since a_ℓ^2 is a quadratic form, any uncertainty in the $a_{\ell m}$ (whether due to coupling, instrument noise, systematic effects and/or foreground sources) produces a positive bias in the estimate of the power spectrum. However, see Górski et al. (1996) and Wright et al. (1996) for spherical harmonic-based analyses that account for these difficulties.

An alternative to estimating the power spectrum is to evaluate its Legendre transform, the 2-point correlation function. For a given power spectrum with multipole amplitudes $C_\ell = \langle |a_{\ell m}|^2 \rangle$, the predicted covariance between pairs of map pixels i and j with angular separation α_{ij} is

$$C(\alpha_{ij}) = \langle T_i T_j \rangle = \frac{1}{4\pi} \sum_{\ell} (2\ell + 1) W_\ell^2 C_\ell P_\ell(\cos \alpha_{ij}) \quad (1)$$

where T_i is the CMB temperature in pixel i , the angled brackets denote an average over an ensemble of universal observers, W_ℓ is the experimental window function that includes the effects of beam smoothing and finite pixel size, and $P_\ell(\cos \alpha_{ij})$ is the Legendre polynomial of order ℓ . We estimate the 2-point correlation function in our sky by evaluating the average product of all map temperatures with a fixed angular separation

$$C(\alpha) = \sum_{i,j} w_i w_j T_i T_j / \sum_{i,j} w_i w_j. \quad (2)$$

where the sum is restricted to pixel pairs (i, j) separated by an angle α , T_i is the observed temperature in pixel i after monopole and dipole (and optionally quadrupole) subtraction, and w_i is the statistical weight of pixel i . This statistic is straightforward to compute, and offers a quick test of the consistency of the power spectrum from map to map.

In the approximation that the 2-point function can be treated as a multivariate Gaussian distribution, one can form a likelihood function with which to estimate the power spectrum normalization. In §2 we present the 2-point correlation data in the 4-year DMR maps and examine its consistency from map to map. In §3 we evaluate the Gaussian likelihood as a function of the mean expected quadrupole moment, Q_{rms-PS} , under the assumption of a scale-invariant, power-law spectrum of anisotropy. In §4 we compare these results with those obtained by other methods and summarize our findings.

2. 2-Point Correlation Data

The 2-point correlation function, as given in Equation 2, is the average product of all pixel temperatures with a fixed angular separation. The data are binned into angular separation bins of width $2^\circ 6$ with the first bin reserved for all pixel pairs (i, j) such that $i = j$, the second bin for pairs with separation between 0° and $2^\circ 6$, and so forth. For the present analysis we employ the maps pixelized in galactic coordinates and use the custom Galaxy cut described by Bennett et al. (1996), for which there are 3881 surviving pixels. To minimize cosmic variance we assign equal weight to each surviving pixel.

The basic 2-point functions obtained from the single frequency maps are shown in Figure 1. We plot both the auto-correlation of the weighted sum of channels A and B at each frequency (the coefficients used to form the weighted average maps analyzed in this paper are given in Table 1) and the cross-correlation between channels A and B. For reference, we also plot, as a solid line, the auto-correlation of the weighted average of all six DMR channel maps. The error bar attached to each point represents the *rms* due to instrument noise, based on 2000 Monte Carlo simulations that include only instrument noise. The plot clearly demonstrates excellent consistency of the 2-point correlations at 53 and 90 GHz, even in the absence of any galactic signal corrections. The 31 GHz data exhibit a small discrepancy from the mean data that is primarily quadrupolar and is presumably due to residual galactic emission.

The data are quantitatively tested for self-consistency by forming differences of the 2-point functions and comparing them to simulations. The statistic for the test is defined as $\chi^2 = (\Delta\mathbf{C} - \langle\Delta\mathbf{C}\rangle)^T \cdot \mathbf{M}^{-1} \cdot (\Delta\mathbf{C} - \langle\Delta\mathbf{C}\rangle)$ where $\Delta\mathbf{C}$ is the observed difference between 2-point functions, with entries $\Delta C_a = C^{(1)}(\alpha_a) - C^{(2)}(\alpha_a)$ (a denotes an angular separation bin, (1) and (2) denote specific data selections), $\langle\Delta\mathbf{C}\rangle$ is the mean difference, computed from simulations described below, and \mathbf{M} is the covariance matrix computed from simulations. For each realization in the Monte Carlo, we generate a single realization of a scale-invariant power-law sky with unit

normalization, and six noise maps, one per channel, with appropriate noise level and coverage (Bennett et al. 1996). We assume the noise is uncorrelated from pixel to pixel, based on the analysis of Lineweaver et al. (1994). It is then possible to generate an ensemble of simulated 2-point functions for any desired auto- or cross-correlation function constructable from the DMR data. We generate such an ensemble for each of the six panels depicted in Figure 1; note that a given realization of the six combinations shares a common CMB signal. We compute χ^2 as defined above for each possible difference and compare its value to the ensemble derived from the simulations. Note that our computation of the covariance matrix from simulations automatically includes bin-bin correlations in the definition of χ^2 . In no case does the observed value of χ^2 exceed the 5% confidence upper limit derived from the simulations, which corroborates the visual consistency of the data.

The 2-point functions obtained from selected multi-frequency combinations of the data are shown in Figure 2. We plot the auto-correlation of the weighted average map, the cross correlation of the 53 and 90 GHz maps, and the auto-correlation of two maps which have had residual, high-latitude galactic emission modeled and removed (Table 1 and Kogut et al. 1996a). Note the excellent consistency between the auto-correlation of the weighted average map, which is sensitive to *all* structure in that map, and the cross-correlation of the 53 and 90 GHz data, which is sensitive only to common structure in the maps. Note also that the two methods used to model and remove high-latitude galactic emission introduce only small changes in the 2-point data, and hence in the angular power spectrum. This observation, coupled with the fact that the Correlation and Combination model maps render very similar 2-point functions, supports the claim of Kogut et al. (1996a) that the free-free emission at high latitudes is 1) weak, and 2) approximately traced by the DIRBE 140 μm map at 7° resolution.

3. Quadrupole Normalization

Given a power law model of initial Gaussian density fluctuations, $P(k) \propto k^n$, where $P(k)$ is the power spectrum of density fluctuations as a function of comoving wavenumber k , it is possible to derive the corresponding angular power spectrum of CMB fluctuations, $C_\ell = \langle |a_{\ell m}|^2 \rangle$ (Bond & Efstathiou 1987). The result is

$$C_\ell = C_2 \frac{\Gamma(\ell + (n - 1)/2)\Gamma((9 - n)/2)}{\Gamma(\ell + (5 - n)/2)\Gamma((3 + n)/2)} \quad (3)$$

For the scale-invariant case, $n = 1$, this reduces to $C_\ell = 6C_2/(\ell(\ell + 1))$, which has one free parameter, the mean quadrupole moment C_2 . We customarily express the normalization in terms of $Q_{rms-PS} \equiv \sqrt{(5/4\pi)C_2}$, the mean *rms* temperature fluctuation expected in the quadrupole component of the anisotropy. We determine the most likely quadrupole normalization, Q_{rms-PS} , from the 2-point function by evaluating the Gaussian approximation to the likelihood function

$$\mathcal{L}(Q_{rms-PS}) \propto \frac{e^{-\frac{1}{2}\Delta\mathbf{C}^T\cdot\mathbf{M}^{-1}\cdot\Delta\mathbf{C}}}{\sqrt{\det(\mathbf{M})}}. \quad (4)$$

Here $\Delta\mathbf{C}^T$ and $\Delta\mathbf{C}$ are m -dimensional row and column vectors with entries $\Delta C_a = C(\alpha_a) - \langle C(\alpha_a) \rangle$, and $\mathbf{M} = \langle (\Delta\mathbf{C})(\Delta\mathbf{C})^T \rangle$ is the covariance matrix of the correlation function. Note that $\Delta\mathbf{C}$ is defined differently than in §2 since we are comparing a single 2-point function to an ensemble here. The angled brackets denote averages over both measurement errors and over the ensemble of anisotropy fields implied by cosmic variance for a given C_ℓ . We estimate the mean correlation and covariance matrix as a function of Q_{rms-PS} using Monte Carlo simulations described above. The simulations account for all important aspects of our data processing including monopole and dipole (and quadrupole) removal on the cut sky. Because of this subtraction, the bins of a given correlation function are not all independent so the covariance matrices derived from the simulations are formally singular. We invert these matrices to form χ^2 using singular value decomposition, which permits an unambiguous identification of the zero modes that arise due to multipole subtraction. We then evaluate the logarithm of the likelihood, $\ln \mathcal{L} = -\frac{1}{2}[\chi^2 + \ln(\det(\mathbf{M})) + const]$, in steps of $1 \mu\text{K}$ in Q_{rms-PS} , spline the result to a resolution of $0.01 \mu\text{K}$, and identify the maximum.

We test the likelihood method for accuracy by feeding the simulated 2-point functions into the likelihood function and solving for an ensemble of Q_{rms-PS} maxima. We define the bias in our method to be $\Delta Q = \langle Q_{max} \rangle - Q_{in}$ where $\langle Q_{max} \rangle$ is the mean of the recovered maxima and Q_{in} is the simulation input normalization. The resulting bias depends on the noise level in the data, but ranges from -0.2 to $-0.4 \mu\text{K}$ for the all cases except the 31 GHz data where it is $\sim -1 \mu\text{K}$. We correct for this bias in all reported results. The uncertainty we assign to Q_{rms-PS} is the *rms* scatter of the ensemble Q_{max} which typically exceeds the *rms* of the Gaussian likelihood by about 10%.

The corrected power spectrum normalization deduced from a variety of data combinations is given in Table 2. The smallest and largest normalization deduced from any data combination are 16.4 and $19.6 \mu\text{K}$ respectively, with values $\sim 18 \mu\text{K}$ generally preferred. The normalization inferred from the 2-point function is now in better agreement with other determinations than was the case with the 2-year data. The change is due to data selection: with the 2-year data, we only analyzed the 53×90 GHz cross-correlation function; with the 4-year data we have analyzed many more data combinations, including the auto-correlation of a weighted average multi-frequency map which yields a normalization $\sim 1.5 \mu\text{K}$ higher than the cross correlation. The multi-frequency auto-correlation is more comparable to the data analyzed by other methods, and the 2-point analysis yields consistent results in that case. For a comparison, see Table 2 of Bennett et al. (1996). In general, the normalization inferred from the 4-year data is slightly less than we found after 2 years, in part because of the extension of the Galaxy cut. For comparison, the 31+53+90 GHz auto-correlation with a straight 20° cut yields a best-fit normalization of $Q_{rms-PS} = 19 \mu\text{K}$. As shown in Table 2, the effects of further modeling and subtraction of galactic emission are less than $1 \mu\text{K}$ in the normalization.

While a likelihood analysis is capable of inferring the best-fit parameters for a given model, it does not say anything *per se* about the goodness of fit. For reference we have included in Table

2 the values of χ^2 at the maximum likelihood value of Q_{rms-PS} (with $n = 1$). Since the 2-point function is only approximately multivariate Gaussian distributed, our tabulated statistic is only approximately χ^2 distributed. However, we have used our Monte Carlo simulations to compute the expected distribution of this statistic and find it to be approximately χ^2 with a mean of ~ 70 and a standard deviation of ~ 12 . The values computed with the DMR data are very consistent with this distribution, implying that the data are well fit by a scale-invariant power spectrum.

4. Conclusions

Analyses of $Q_{rms-PS|n=1}$ have also been reported by Banday et al. (1996), Górski et al. (1996), Hinshaw et al. (1996), Kogut et al. (1996b), and Wright et al. (1996). All results lie between 15.5 and 19.6 μK with most between 17.5 and 18.5 μK . In general, all methods for analyzing a given data combination give consistent results, while there is modest dependence on data selection. Fortunately, the dependence on data selection does not exceed the statistical uncertainty due to cosmic variance and instrument noise. A reasonable conclusion to draw for the normalization of a scale invariant spectrum is $Q_{rms-PS|n=1} = 18 \pm 1.6 \mu\text{K}$, with the error quoted conservatively.

We gratefully acknowledge the many people who made this paper possible: the NASA Office of Space Sciences, the *COBE* flight operations team, and all of those who helped process and analyze the data.

Table 1. DMR Map Combination Coefficients^a

Map	31A	31B	53A	53B	90A	90B	DIRBE	Haslam
31ws	0.611	0.389	0	0	0	0	0	0
53ws	0	0	0.579	0.421	0	0	0	0
90ws	0	0	0	0	0.382	0.618	0	0
53+90	0	0	0.412	0.299	0.110	0.179	0	0
31+53+90	0.049	0.032	0.378	0.275	0.102	0.164	0	0
Correlation ^b	0.049	0.032	0.378	0.275	0.102	0.164	3.364	0.314
Combination ^c	−0.185	−0.117	0.367	0.266	0.256	0.413	2.055	−0.170

^aThe maps are formed using the above coefficients according to the prescription: $\sum_i C_{DMR}^i T_{DMR}^i - C_H T_H - C_D T_D$, where $i = 31A, \dots, 90B$ is a channel index, C_{DMR}^i are the DMR map coefficients given above, T_{DMR} are the DMR maps in μK of thermodynamic temperature, C_H is the coupling coefficient to the Haslam map, in $\mu\text{K} / \text{K}$, given above, T_H is the Haslam map, in K , C_D is the coupling coefficient to the DIRBE 140 μm map, in $\mu\text{K} / (\text{MJy}/\text{sr})$, given above, and T_D is the DIRBE 140 μm map, in MJy/sr . The resulting map has units of μK , thermodynamic.

^bThe coefficients give the most sensitive combination of the 31, 53 and 90 GHz data, in thermodynamic units. The Haslam map is used to model synchrotron emission, it was fit to the DMR data under the assumption that its spectral index was $\beta_s = -3.0$. The DIRBE 140 μm map is used to model both free-free and dust emission, see Kogut et al. (1996a). The free-free component was fit assuming a spectral index $\beta_{ff} = -2.15$, the dust component was fit assuming $\beta_d = +2.0$. The coefficients given above combine the free-free and dust emission.

^cThe coefficients give the most sensitive combination of the 31, 53 and 90 GHz data, in thermodynamic units, consistent with the constraint that emission with a spectral index $\beta_{ff} = -2.15$ (free-free emission) be nullified. The Haslam map is used to model synchrotron emission, as above. The DIRBE 140 μm map is used to model dust emission, as above.

Table 2. Scale-invariant Power Spectrum Normalization

Map #1 ^a	Map #2 ^a	$\ell_{min} = 2^b$ $Q_{rms-PS} \text{ (}\mu\text{K)}$	χ^2	$\ell_{min} = 3$ $Q_{rms-PS} \text{ (}\mu\text{K)}$	χ^2
Single frequency cross-correlation					
31A	31B	18.2 ± 4.1	68.3	18.0 ± 4.6	71.0
53A	53B	18.3 ± 1.6	73.5	18.6 ± 1.7	69.6
90A	90B	16.4 ± 2.2	72.3	18.4 ± 2.3	71.0
Single frequency auto-correlation					
31ws	31ws	17.1 ± 3.7	67.9	17.6 ± 4.0	79.6
53ws	53ws	18.7 ± 1.6	99.9	19.4 ± 1.6	97.5
90ws	90ws	17.5 ± 2.0	63.5	19.0 ± 2.2	61.5
Multi-frequency cross-correlation					
53ws	90ws	17.2 ± 1.5	60.8	17.8 ± 1.5	64.1
53ss	90ss	17.0 ± 1.6	61.2	17.9 ± 1.6	62.3
Multi-frequency auto-correlation					
53+90	53+90	18.5 ± 1.4	84.2	19.6 ± 1.5	83.5
31+53+90	31+53+90	18.6 ± 1.4	80.0	19.3 ± 1.4	78.2
Multi-frequency auto-correlation with Galaxy model					
Correlation	Correlation	17.5 ± 1.4	76.2	18.5 ± 1.4	78.3
Combination	Combination	16.7 ± 2.0	89.2	17.8 ± 2.2	92.4

^aThe coefficients that comprise the map combinations in these columns are given in Table 1, except for 53ss and 90ss which are straight sum maps: (A+B)/2.

^b ℓ_{min} is the lowest order multipole remaining in the map after subtracting a best-fit multipole of order $\ell_{min} - 1$. Q_{rms-PS} is the most-likely quadrupole normalization, after calibrating the likelihood with Monte Carlo simulations. χ^2 is tabulated, for reference, with respect to the mean of a scale-invariant model with the corresponding most-likely normalization. There are 71 bins in the 2-point function.

REFERENCES

- Banday, A.J., et al. 1996, ApJ, in preparation
- Bennett, C.L., et al. 1992, ApJ, 396, L7
- Bennett, C.L., et al. 1994, ApJ, 436, 423
- Bennett, C.L., et al. 1996, ApJ, submitted
- Bond, J.R., & Efstathiou, G. 1987, MNRAS, 226, 655
- Górski, K.M., Hinshaw, G., Banday, A.J., Bennett, C.L., Wright, E.L., Kogut, A., Smoot, G.F., & Lubin, P. 1994, ApJ, 430, L89
- Górski, K.M., Banday, A.J., Bennett, C.L., Hinshaw, G., Kogut, A., Smoot, G.F., & Wright, E.L. 1996, ApJ, submitted
- Hinshaw, G., Banday, A.J., Bennett, C.L., Górski, K.M., Kogut, A., Smoot, G.F., & Wright, E.L. 1996, ApJ, submitted
- Kogut, A., et al. 1992, ApJ, 401, 1
- Kogut, A., Hinshaw, G., Banday, A.J., Bennett, C.L., Górski, K.M., Smoot, G.F., & Wright, E.L. 1996a, ApJ, submitted
- Kogut, A., Banday, A.J., Bennett, C.L., Górski, K.M., Hinshaw, G., Smoot, G.F., & Wright, E.L. 1996b, ApJ, submitted
- Lineweaver, C.H., et al. 1994, ApJ, 436, 452
- Smoot, G.F., et al. 1992, ApJ, 396, L1
- Wright, E.L., et al. 1992, ApJ, 396, L13
- Wright, E.L., Smoot, G.F., Bennett, C.L., & Lubin, P.M. 1994, ApJ, 436, 443
- Wright, E.L., Bennett, C.L., Górski, K.M., Hinshaw, G., & Smoot, G.F. 1996, ApJ, submitted

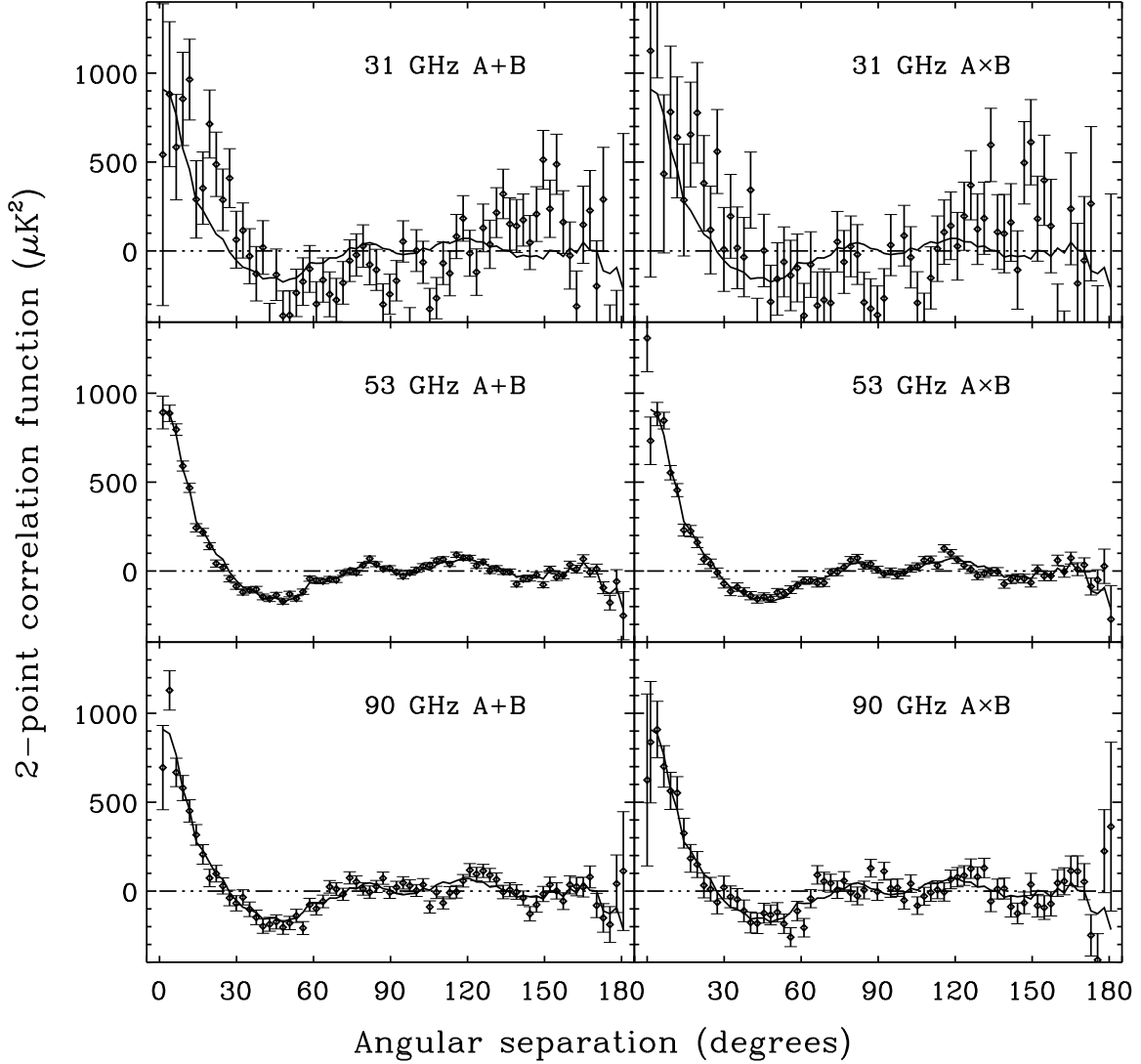


Fig. 1.— 2-point correlation functions obtained from the individual frequency maps, after monopole and dipole subtraction. The left-hand panels show the auto-correlation functions obtained from a weighted average of the A and B channel maps. The right-hand panels show the cross-correlation of the A and B channels, which are sensitive only to common structure in the maps. The error bars represent the uncertainty due to instrument noise, as described in the text. To guide the eye, the solid line is the auto-correlation of the weighted average of all six channels maps. All six 2-point functions are statistically consistent with each other.

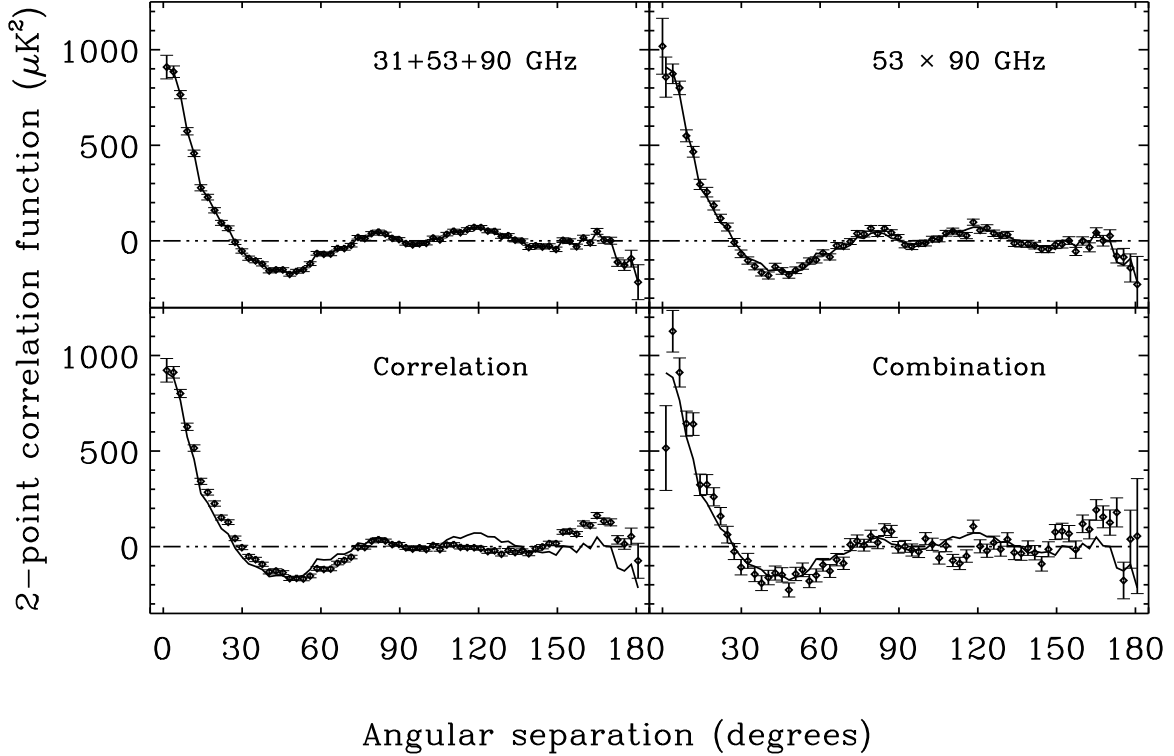


Fig. 2.— 2-point correlation functions obtained from the multi-frequency maps after monopole and dipole subtraction. *top left*) The auto-correlation function of the weighted average map constructed from all six DMR channels. *top right*) The cross correlation function of the 53 GHz weighted sum map with the 90 GHz weighted sum map. *bottom left*) The auto-correlation function of the weighted average map with best-fit Galaxy template maps subtracted from the map (Kogut et al. 1996a). *bottom right*) The auto-correlation function of the linear combination map designed to cancel free-free emission. This map has a best-fit model of the synchrotron and dust emission also subtracted. In all panels the error bars represent the uncertainty due to instrument noise, as described in the text. To guide the eye, the solid line is the auto-correlation of the weighted average map (top left panel).